ELSEVIER

Optics and Lasers in Engineering 41 (2004) 827–847

OPTICS and LASERS in ENGINEERING

Fabrication of high-aspect-ratio microstructures using excimer laser

Ampere A. Tseng[a,*], Ying-Tung Chen[b], Kung-Jeng Ma[b]

[a] *Department of Mechanical and Aerospace Engineering, Arizona State University, P.O. Box 876106, Tempe, Arizona 85287-6106, USA*

[b] *Department of Mechanical Engineering, Chung Cheng Institute of Technology, Tashi, Taiwan, ROC*

Received 14 February 2003; accepted 16 May 2003

Abstract

An excimer laser micromachining system is developed to study the ablation of high-aspect-ratio microstructures. The study examines the ablation efficiency, specifically, the impact of changing major laser operating parameters on the resulting microstructural shapes and morphology. The study focuses on glass, although results on silicon and aluminum are also included for comparison. In ablating grooved structures, the ablation depth has been observed to be linearly proportional to the operating parameters, such as the pulse number and fluence. The results specifically indicate that ablation at low fluence and high repetition rates tends to form a V-shaped cross-section or profile, while a U-shaped profile can be obtained at high fluence and low repetition rate. The ablation rate or ablated volume has then been quantified based on the ablation depth measured and the ablated profile observed. The threshold fluence has also been obtained by extrapolating experimental data of ablation rate. The extrapolation accuracy has been established by the good agreement between the extrapolated value and the one predicted by Beer's law. Moreover, a one-dimensional analytical solution has been adopted to predict the ablated volume so as to compare with the experimental data. The reasonable agreement between the two indicates that a simple analytical solution can be used for guiding or controlling further laser operations in ablating glass structures. Finally, the experimental results have shown that increasing the repetition rate favors the morphology of ablated surfaces, though the effect of repetition rate on ablation depth is insignificant.

Keywords: Ablation; Ablation rate; Excimer laser; Fluence; Glass substrate; Microgroove

*Corresponding author. Fax: +1-480-965-1384.
E-mail address: ampere.tseng@asu.edu (A.A. Tseng).

0143-8166/03/$ - see front matter
doi:10.1016/S0143-8166(03)00062-9

1. Introduction

Excimer lasers are pulsed gas lasers that use a mixture of gases to provide emission at a series of discrete wavelengths in the UV region of the spectrum. The word "excimer" is a contraction of the term "excited dimer". This describes a diatomic molecule that is bound in its electronically excited upper state, but is repulsive or only weakly bound in its lower ground state. Excimer lasers are increasingly being used for machining micro-structures and devices [1,2]. In micromachining, excimer lasers remove the material from a substrate through an ablation mechanism. They are capable of making microstructures with feature sizes on the order of 1 μm and they are applicable for all kinds of materials, including polymers, metals, and ceramics [3,4].

Ablation can be one or a mix of two processes: "photothermal" and "photochemical". A photochemical or electronic process is often referred to as a non-thermal process because the removal of material is caused by a direct breaking of atomic bonds as energy is absorbed. In contrast, the absorbed laser energy is converted to lattice vibrational energy (thermal) to melt and vaporize the material in a photothermal process. To directly break atomic bonding, the intensity of the laser beam should be higher than a threshold value, which is mainly dependant on the material to be ablated and the wavelength of the laser. At intensities below the ablation threshold, the absorbed energy heats the substrate and raises the substrate temperature higher than its boiling or sublimation point. Consequently, the material begins to liberate. Both the photothermal and photochemical processes liberate molecular-sized material from the surface. The two processes can occur in varying degrees of combination in micromachining that uses high-intensity excimer lasers [5,6].

The photochemical process normally dominates for ablation of polymers, which have relatively low thresholds, while the photothermal process dominates for ablation of ceramics and metals, which possess high thresholds [7,5]. The typical feature size created by a photothermal process is larger than that produced by a photochemical process, and the temperature profile resulting from this thermal process can often produce extensive damage in the heat-affected zone surrounding the melted or vaporized region. By minimizing the heat-affected zone or the undesired thermal effect, a feature size in microscale levels can be accomplished. Thus, the photochemical process is preferred in micromachining. Also, since the ablation depth per pulse is often greater than the optical absorption depth and the pulse length is far shorter than the thermal diffusion time scale, the amount of residual energy left in the substrate is typically small.

Since the laser technology has improved substantially over the past decade, excimer lasers now possess relatively high pulse energies, short pulse lengths, and high average and peak powers as compared to other laser sources. These attributes make them the most efficient and popular ablation tool as well as a powerhouse for micromachining applications. One of the most widely known applications is the inkjet-printer nozzle, which is a successful commercialized product in the area of microscale fluidic devices. In addition to many other industrial applications recently,

laser micromachining has also been successfully applied to many medical or clinical processes, such as retinal photocoagulation, angioplasty, corneal sculpting, and cartilage or nerve treatment [3,4].

To further enhance the applications of excimer lasers, a better understanding of the nature of their micromachining process is required. In the present study, an Argon–Fluorine (ArF) excimer laser is selected because of its short wavelength. A laser projection system is developed to ablate high-aspect-ratio microstructures. The study examines the ablation efficiency through experiments and analytical models. Specifically, the impact of varying major operating parameters, including pulse fluence, pulse repetition rate, and pulse number, on the resulting microstructural shapes and morphology is studied. The threshold fluence is also studied using both experimental data and theoretical prediction. Finally, recommendations are included for future improvement of ablation process by excimer laser.

2. Experiment setup

The laser micromachining workstation for the present study consists of an ArF excimer laser source, an optical set, a moving stage, a mask holder, an optical table, and an outer protective shielding as shown in Fig. 1. The ArF laser has the shortest wavelength, 193 nm, in the excimer laser family commonly used by the industry. The laser source is the Model LPX210 manufactured by Lambda Physik (Germany). During operation, the workstation is kept in a temperature controlled environment ($\pm 2^{\circ}$C typically) to reduce errors due to thermal expansion of mechanical systems. A shielding that can completely absorb the 193 nm UV laser light is built to protect the safety of the operators.

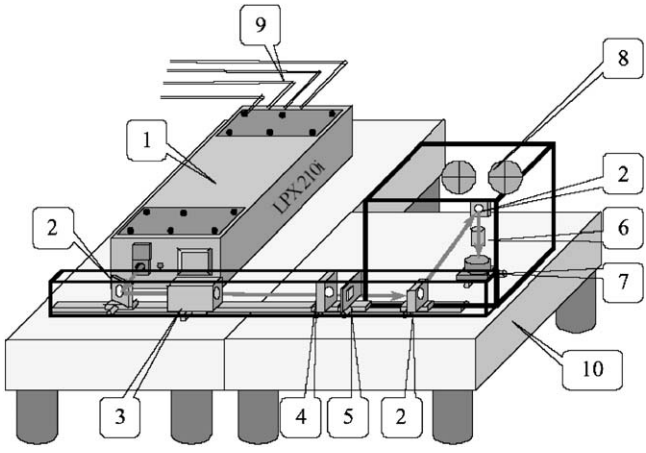

Fig. 1. ArF excimer laser micromachining system: (1) laser source (2) 45° mirror (3) homogenizer (4) condenser lens (5) mask (6) focus lens (7) moving stage (8) air conditioner (9) laser gas (10) optical table.

The workstation can perform both projection printing and direct writing. Only projection printing is considered for the present study. The essence of a projection printing system is the ability to illuminate the mask with a uniform fluence, which relies entirely upon the uniformity of the laser beam itself. In the present projection system, the beam is conditioned to achieve a uniform energy distribution at the object plane, using a 7×7 fixed-array homogenizer. The homogenizer produces a 12×23 mm uniform illumination at the mask plane with an intensity variation less than $\pm 5\%$ RMS. Projection lenses of various magnifications are used to transfer the pattern of the mask onto the sample, which is mounted on a precision air-bearing XY stage. The 7×7 fixed-array homogenizer, made by MicroLas (Germany), provides a 40% transmission rate for the laser light and transforms a Gaussian laser beam energy distribution to a uniform distribution. The projection and focus lenses are made of UV grade fused silica, provided by CVI (USA) with a resolution better than 2.0 μm, a focus depth of 14.0 mm and 90% transmission rate at a wavelength of 193 nm.

In the present setup for projection printing, a mask having slot-shaped openings is used to quantify micromachining characteristics. The mask is made of 200-μm thick 304 stainless steel and is chemically etched to produce 200-μm wide slots. The projection lens has a $10\times$ demagnification and a maximum field size of 1.2×2.3 mm can be obtained based on the 12×23 mm beam source from the homogenizer. Thus, the slot pattern printed onto the sample is expected to be 20 μm wide. During ablation, the maximum fluences or energy densities at the sample with the $10\times$ lenses are kept at values lower than 2.5 J/cm^2; the corresponding maximum fluence provided at the mask is below 0.025 J/cm^2 and should not cause any damage to the mask. The conventional chrome-on-quartz mask can also be used because the UV grade fused quartz has a transmission rate higher than 90% at a wavelength of 193 nm.

The ranges of the operating parameters, including repetition rate, pulse number, fluence (energy density), and duration time, are listed in Table 1. The duration of each pulse is fixed at 20 ns. The specific values of the operating parameters can all be preset by a PC-base controller. To guarantee high machining quality, the focus distance must be readjusted according to each sample thickness to preserve perpendicular contact between the laser beam and the sample surface. During ablation, the positioning stage can move in both X and Y directions and rotate about the θ-axis. The Z-axis movement is for finer focus adjustment. The XY plane is always kept perpendicular to the laser beam during operation. The workstation

Table 1
Operating parameters of laser ablation

Parameter (units)	Range
Fluence (J/cm^2)	1.4, 1.7, 2.1, 2.4
Duration time (ns)	20
Repetition rate (Hz)	1, 2, 5, 10
Pulse number	50, 100, 150, 200, 250

enclosure and frame are all mounted on an optical table equipped with a vibration isolation system, which reduces vibration induced by the ambient environment during operation.

3. Results and discussions

The material considered is borosilicate glass (BK7), supplied by VWR Scientific. Single-crystal silicon and 2024 aluminum are also evaluated, but their results are merely used for comparison. The typical sample size used in the present study is 25 mm^2 in area and 0.2 mm in thickness. After machining, an oxide layer or debris is often accumulated on the machined surface and must be discarded, so that it does not erroneously affect sample analysis or measurements. A solution of 10% HF and 90% distilled water can effectively clean the debris. After cleaning, the machined profiles are measured and examined. The duration of each pulse in all of the experiments is set at 20 ns.

3.1. Effects of material properties

The ablation characteristics are primarily dictated by the laser/material interactions as well as the laser parameters, especially the fluence, repetition rate, pulse number, and duration time. Fig. 2 shows the scanning electronic microscope (SEM) micrographs of the surface morphology of the three materials after ablation at a fluence of 2.4 J/cm^2 and a repetition rate of 10 Hz with two different pulse numbers, 150 and 250. The micrographs were taken by a Philips Model 515 SEM. Since glass is a dielectric material, a thin gold film (3–5 nm thick) is coated on the ablated glass sample by vacuum evaporation to make it conductive for SEM observation. As shown in the figure, the ablation depth of aluminum or silicon is less than that of glass. Also, the trench surface of either aluminum or silicon is more irregular than that of glass.

As mentioned earlier, since the threshold values of both metals and ceramics are relatively high, the ablation of these materials is primarily a thermal or photothermal process. Consequently, their associated thermal properties are important in the interpretation of their ablation results. Based on the material properties shown in Table 2, the melting temperature of aluminum is relatively low (660°C) as compared to silicon (1410°C), and its thermal conductivity (238 W/m K) is higher than both glass (1.1 W/m K) and silicon (157 W/m K). Thus, the heat converted by laser energy does not accumulate fast enough to melt aluminum. Consequently, the ablation depth of aluminum is smaller than that of glass, and the thermally affected surface of the machined or ablated grooves is more irregular. The thermal conductivity of silicon (157 W/m K) is lower than that of aluminum, but it has a higher melting temperature (1410°C). The combination of these two properties makes silicon's ablation rate or depth similar to that of aluminum. On the other hand, not only the thermal conductivity of glass (1.1 W/m K) is significantly lower than those of silicon and aluminum, but also its glass-transition temperature (820°C)

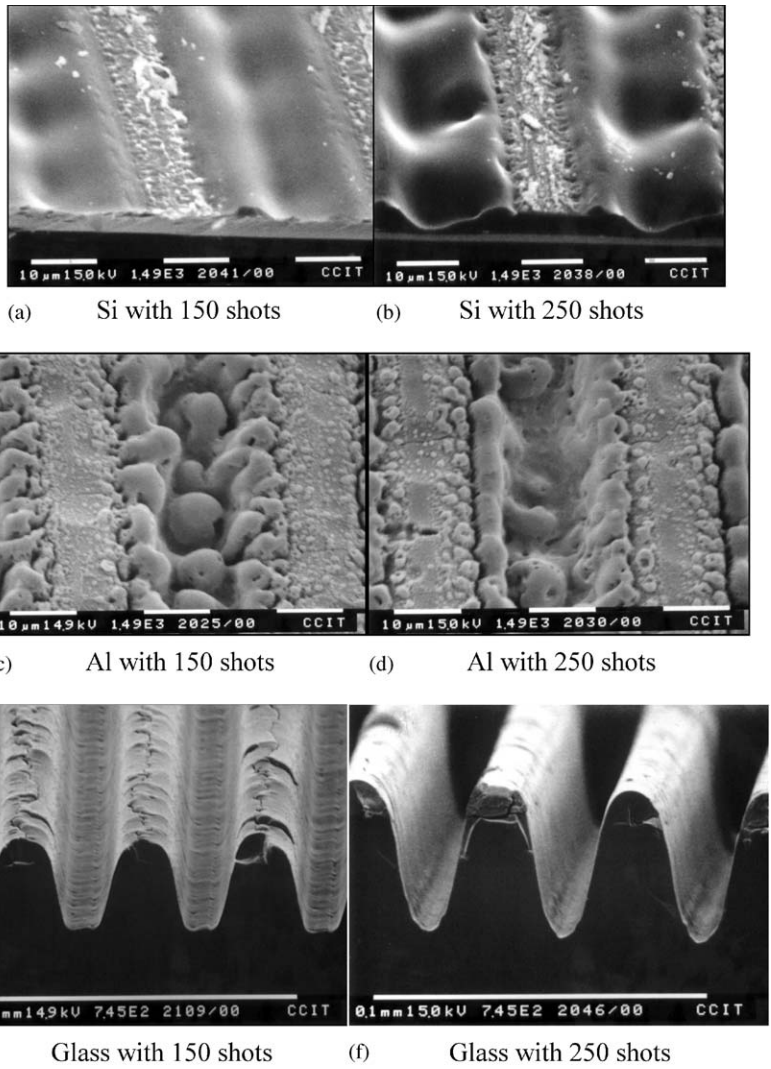

Fig. 2. Surface morphologies of three materials after ablation at a fluence of 2.4 J/cm^2.

is much lower than the melting temperature of silicon and comparable to that of aluminum. As a result, glass appears to have the best ablation efficiency or rate among the three materials evaluated, and should be a good candidate for laser processing.

3.2. Ablation rate

The effects of the pulse repetition rate, pulse number, and fluence on the ablation rate or depth of glass are studied in this section. Three repetition rates of 2, 5, and

Table 2
Thermophysical properties of glass, aluminum, and silicon[a]

Properties		Glass	Aluminum	Silicon
Density	ρ_s (kg/m^3)[b]	2230	2700	2330
	ρ_l (kg/m^3)	2030	2385	2130
Heat Capacity	C_s (J/kg K)	712	917	716
	C_l (J/kg K)	1200	1080	1200
Thermal Conductivity	k_s (W/mK)	1.10	238	157
	k_l (W/mK)	2.87	100	30
Melting Temperature	T_m (°C)	820	660	1410
Absorptivity	A_s	0.8	0.059	0.02
	A_l	0.8	0.064	0.05

[a] Based on data in [8–11].
[b] The subscripts, S and L, represent solid and liquid phases, respectively.

10 Hz are considered. The relationships between the ablation depth and the pulse number for the three repetition rates are plotted in Figs. 3–6 for fluences of 1.4, 1.7, 2.1, and 2.4 J/cm^2, respectively. The ablation depth is measured directly from the SEM images, as shown in Fig. 7. The span or opening of the ablated grooves or trenches is approximately 20 μm; this figure is expected since the slot width on the 10 × mask is 200 μm and the slot pattern printed onto the sample should be 20 μm wide. From the data shown in Figs. 3–6, the ablation depths for all four fluences considered increase quite linearly with the pulse number. This linear relationship is consistent with the results obtained by Kautek et al. [12], who used a focused laser beam to machine barium–aluminum–borosilicate glass. They believed that the linearity is resulted from the vaporized material that has left the cavity without redeposition. Note that the increment of input energy is linearly proportional to the increment of pulse number.

The impact of repetition rate is somewhat interesting. As shown in Figs. 5 and 6, the ablation depth for a fluence larger than 2.1 J/cm^2 is the smallest at 10 Hz and the largest at 2 Hz. On the other hand, the ablation depth is the smallest at 2 Hz and the largest at either 5 or 10 Hz for a fluence lower than 1.4 J/cm^2 as shown in Figs. 3 and 4. As mentioned earlier, laser ablation on glass is dominated by photothermal reactions. The absorbed laser energy can neither reach the ablation threshold nor heat the glass to its melting or vaporized state at lower fluences. Therefore, it is necessary to have a high repetition rate in order to accumulate sufficient amount of energy to ablate the glass. If the repetition rate is relatively low, the absorbed energy may have more time to transfer to the adjacent region, leading to slower thermal accumulation. This means that an ablation is still possible but more applied pulses are needed. If the repetition rate is high, thermal accumulation can be faster and fewer pulses are needed to ablate the materials. However, this still cannot fully explain the fact that the results at lower fluences have the largest ablation at either 5 or 10 Hz. A further investigation into this matter is encouraged.

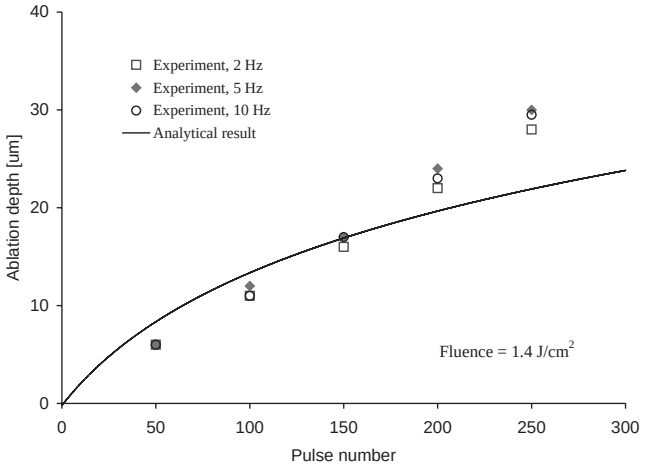

Fig. 3. Effect of pulse number and repetition rate on ablation depth at fluence = 1.4 J/cm^2.

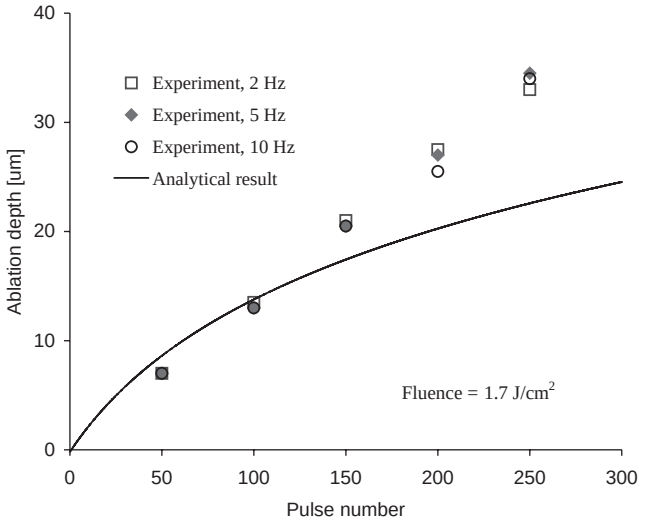

Fig. 4. Effect of pulse number and repetition rate on ablation depth at fluence = 1.7 J/cm^2.

It is also noted that all of the differences between the highest and lowest ablation depths are relatively small, less than 10%. It is suspected that since glass has very low thermal conductivity and diffusivity, the amount of heat transferred to the neighboring region between pulses is minimal and the repetition rate or the time between ablation pulses plays a very minor role in the ablation of glass. As a result, the cases where the highest ablation rate occurs at 5 Hz should not be caused by thermal related factors.

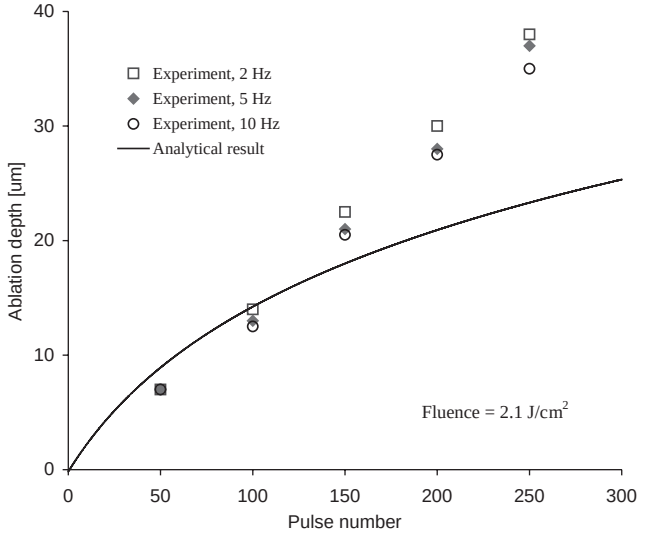

Fig. 5. Effect of pulse number and repetition rate on ablation depth at fluence = 2.1 J/cm^2.

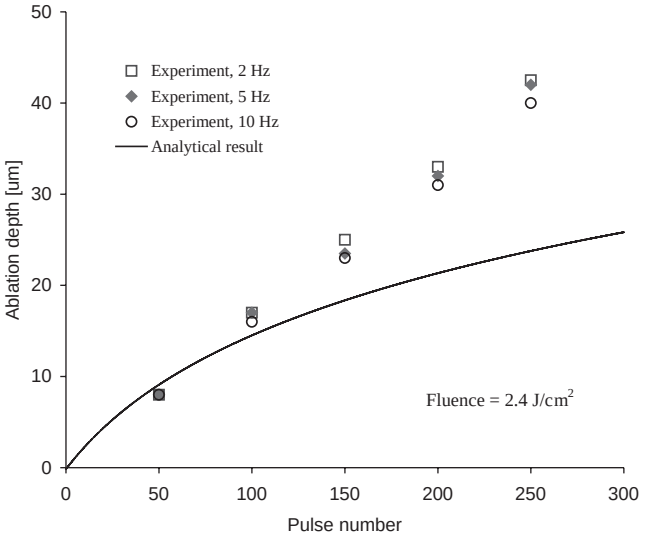

Fig. 6. Effect of pulse number and repetition rate on ablation depth at fluence = 2.4 J/cm^2.

The mathematical correlation between the ablation depth and the pulse number is also obtained. Fig. 8 shows the correlation for four different fluences at a repetition rate of 5 Hz. The experimental data fit the correlation curves very well; the relationship is indeed linear and all of the curves pass through the origin, which means that each pulse at a specific fluence contributes equally to the ablation depth.

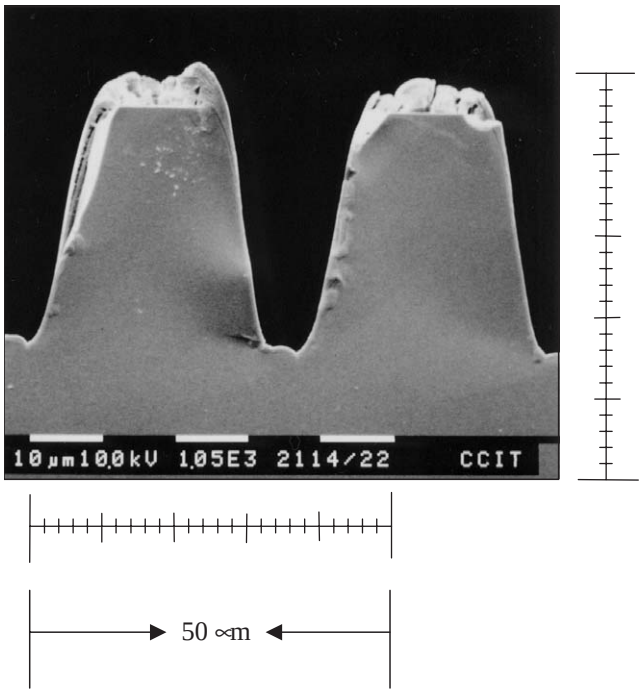

Fig. 7. Measurement of ablation depth.

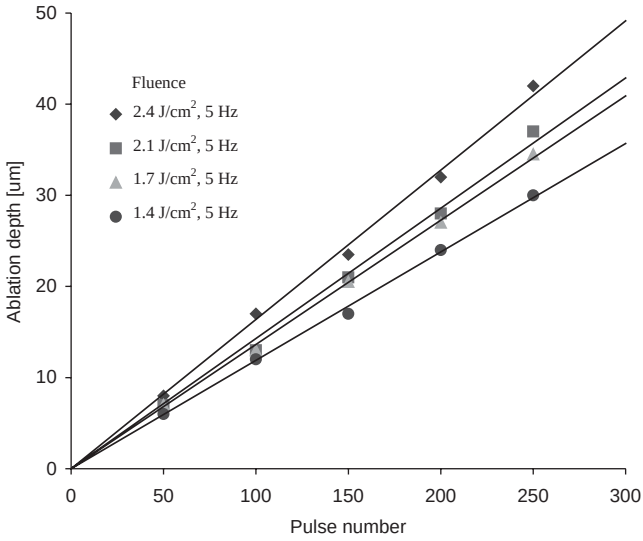

Fig. 8. Mathematical correlations between the ablation depth and pulse number at various fluences.

The corresponding slopes for fluence at 1.4, 1.7, 2.1, and 2.4 J/cm^2 are 0.119, 0.136, 0.143, and 0.164 μm, respectively. Physically, the slope represents the ablation depth rate (per pulse). The slope values obtained further attest our earlier inference that the larger the fluence, the higher the ablation rate. Note that the correlation coefficients for each curve fitting shown in Fig. 8 are all higher than 0.99, which means the ablation depth correlates with the pulse number almost perfectly. The coefficient R is used to gauge the accuracy of correlation and always lies between -1 and $+1$. A value of zero occurs when the two variables are totally independent of each other, while it reaches 1 when the two variables correlate perfectly, i.e., no deviation from the linear curve [13].

3.3. Threshold fluence

The information on threshold fluence of ablation can also be explored from the experimental data. If the ablation depth data are plotted against the fluence in a log scale, the corresponding fluence at zero ablation depth is the threshold fluence. Fig. 9 shows that the average threshold fluence obtained from five different pulse numbers with a fixed repetition rate of 5 Hz is 0.263 J/cm^2, with a standard deviation of 0.05 J/cm^2. Although the inaccuracy or relative standard deviation is as high as 15%, the estimated values with relatively high deviations are expected and reasonable because the threshold fluence and ablation rate are strongly dependent on the surface conditions and an accurate prediction of these values is difficult, especially for ceramics [5]. Also, the threshold value is extrapolated from several extrapolated experimental lines; consequently, the inaccuracy from double or indirect extrapolation should be higher.

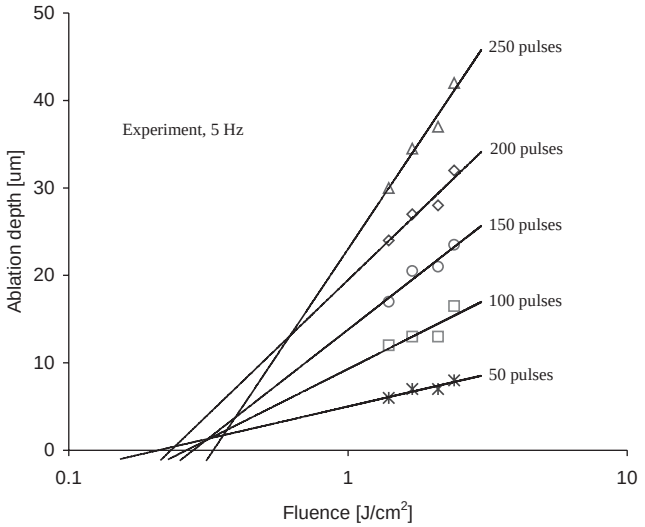

Fig. 9. Extrapolation to threshold influences at various pulse numbers.

The accuracy of the threshold value just obtained will be further studied by comparing it with the value calculated by the well-known Beer's law:

$$\Delta d = \ln(F_i/F_t)/\alpha, \tag{1}$$

where Δd is the ablation depth per pulse, α is the absorption coefficient, F_i and F_t are the incident and threshold fluences, respectively. If the threshold value of $0.263\ \mathrm{J/cm^2}$ is reliable, it can be used to predict Δd by Beer's law shown in Eq. (1). The predicted Δd should be consistent with the one extrapolated from the experimental data shown in Fig. 8.

It is somewhat surprising that the absorption coefficient (α) of BK7 glass at a wavelength (λ) of 193 nm is not available in many sources searched. As an alternative, the α data at λ from 400 to 300 nm are used to extrapolate the value at $\lambda = 193$ nm. Fig. 10 shows the extrapolation and the 10 values in circles are obtained from the optical/laser handbook of Nikogosyan [10] and the extrapolated α at $\lambda = 193$ nm is $13,400\ \mathrm{cm^{-1}}$. Substituting the values of α ($13,400\ \mathrm{cm^{-1}}$) and F_t ($0.263\ \mathrm{J/cm^2}$) into Eq. (1), Δd for fluences at 1.4, 1.7, 2.1, and $2.4\ \mathrm{J/cm^2}$ are calculated as 125, 139, 155, and 165 nm/pulse, respectively. As shown in Fig. 11, the calculated values agree very well with those based on the experimental data from Fig. 8. Also Fig. 11 shows that based on the measured data of Δd, F_t is found to be $0.29\ \mathrm{J/cm^2}$ and agrees with the original value of $F_t = 0.263\ \mathrm{J/cm^2}$ within 10%. The consistency shown in Fig. 11 further demonstrates the fact that the threshold fluence ($= 0.263\ \mathrm{J/cm^2}$) extrapolated from the experimental data is reliable and accurate.

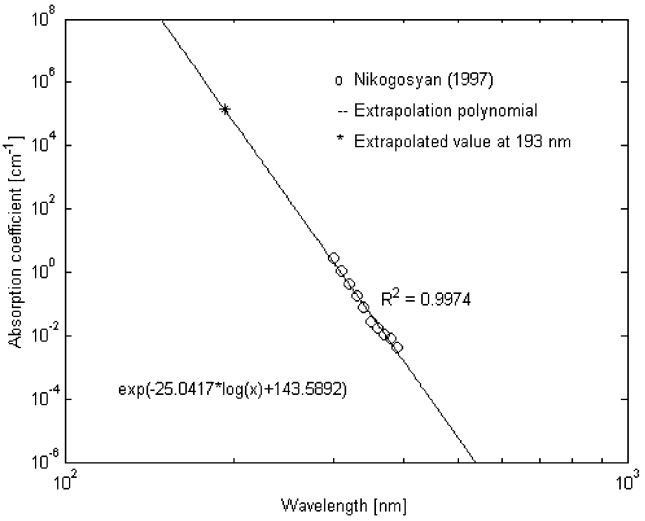

Fig. 10. Extrapolation of absorption coefficient at a wavelength of 193 nm.

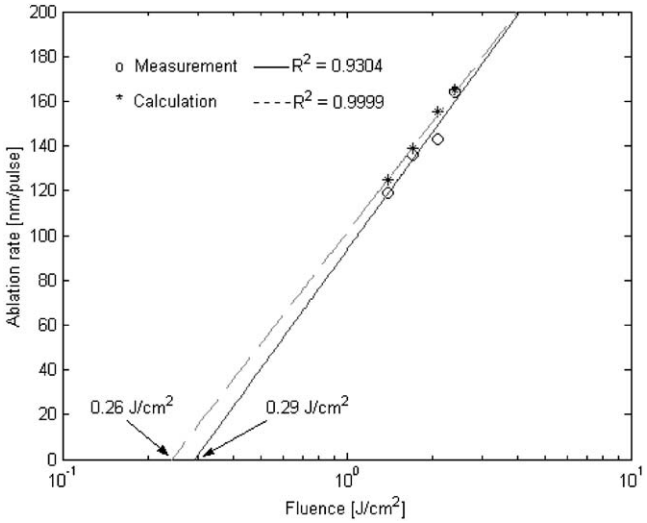

Fig. 11. Comparison of prediction and experimental data on ablation depth per pulse at various fluences.

3.4. Ablated trench shapes and morphology

As a laser beam strikes a target, the target material is rapidly melted and partially vaporized. In glass, the photothermal effect is dominant. If the vaporized elements are continuously bombarded by the subsequent laser beams (or photons), their temperatures keep rising and the vaporized elements eventually ionize to plasma. The ionized vapor or plasma can continuously absorb the rest of laser energy and rapidly expand outward, forming plasma pressure waves [5]. The lifetime or duration of plasma state is very short, on the order of femtoseconds [14], and the plasma waves will not interact with those of subsequent laser pulses because the repetition rate in the present experiment is only 1 Hz. Concurrently, this high vapor- and ion-pressure build-up can sputter away melted materials to form fine droplets, resulting in small cavities in the target material, as shown in Fig. 12. The forming of small cavities and sputtering droplets is a major material-removing mechanism in laser ablation.

In glass ablation, these small cavities can form into trenches or grooves of various shapes by changing the pulse fluence and number. It has been found that for the first few dozens of pulses, the fluence does not affect the ablated shape much, as shown in Fig. 13 for a pulse number of 50. As the number of pulses increases, the cross-sectional profile produced by high fluences (2.1 and 2.4 J/cm^2) is U-shaped, and the one produced by low fluences (1.4 J/cm^2) becomes V-shaped, as shown in Fig. 14 for a pulse number of 200. At lower fluence levels, glass is partially fluidized and a small part of fluidized material is vaporized. Under repetitious pulses, the thermal energy is persistently absorbed in the region directly struck by the laser, and it also slowly transfers to the surroundings due to the low conductivity of glass. As a result, the

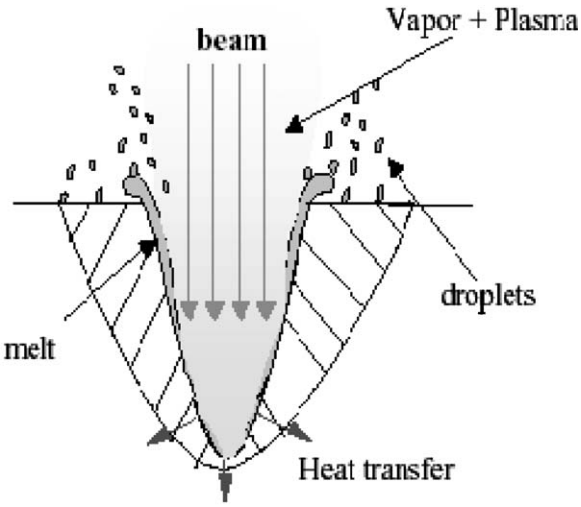

Fig. 12. Formation of vapor/plasma and sputtering of molten-droplet in laser ablation.

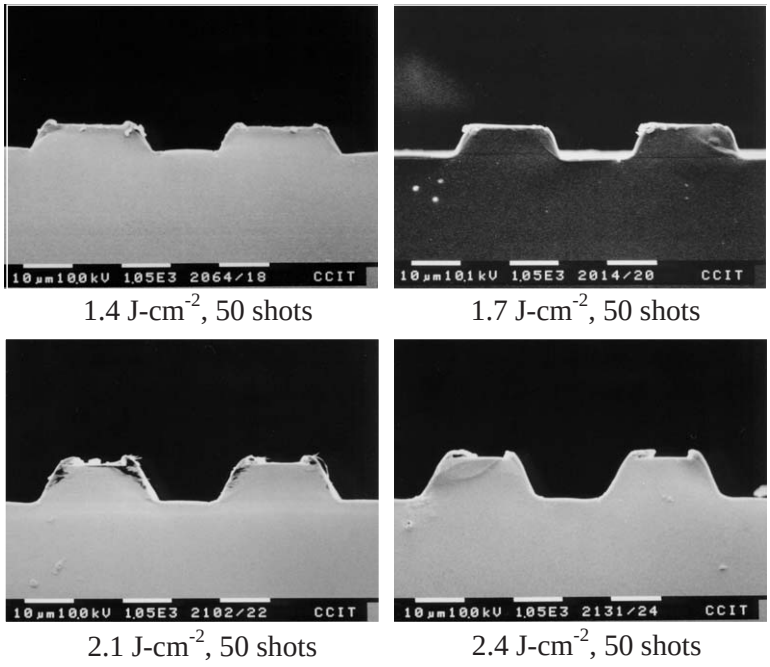

Fig. 13. Effect of fluence on shape of ablated glass at 50 shots.

central region has a higher temperature than that of the adjacent regions. The central region that accumulates more energy is sputtered sooner than the adjacent regions, which results in a V-shaped profile since the central region is always ablated first. In

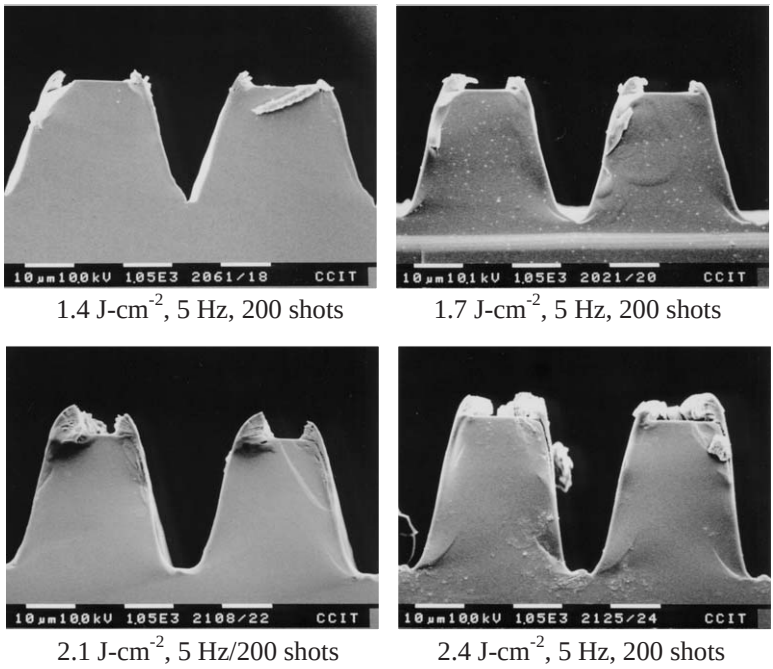

1.4 J-cm^{-2}, 5 Hz, 200 shots 1.7 J-cm^{-2}, 5 Hz, 200 shots

2.1 J-cm^{-2}, 5 Hz/200 shots 2.4 J-cm^{-2}, 5 Hz, 200 shots

Fig. 14. Effect of fluence on shape of ablated glass at 200 shots.

contrast, at higher fluences (2.1 and 2.4 J/cm^2), the energy accumulates faster and a larger amount of fluidized glass is vaporized. Thus, a higher vapor or plasma pressure can build up inside the groove to sputter materials more evenly along the periphery (wall) of the groove, resulting in a U-shaped profile. Fig. 15 clearly notes the profile changes from V-shaped to U-shaped as the fluence increases from 0.6 to 2.4 J/cm^2.

Fig. 16 shows the ablated morphology and shapes at three different repetition rates for pulse numbers of 100 and 200 shots. A lower pulse repetition rate (1 Hz) leads to rougher surfaces with a waved appearance, while a higher pulse repetition rate results in smoother surfaces featuring more compact and finer residual debris. Similar results are also observed in ablating silicon. As shown in Fig. 17, the higher the pulse repetition rate (10 Hz), the finer the ablated surfaces. There is a reasonable explanation for these observations. At lower repetition rates, there is sufficient time for the sputtered droplets to integrate with the neighboring droplets to form bigger droplets or debris, which can be cooled down and solidified on the surface of the groove, resulting in a rougher surface. On the other hand, at higher pulse repetition rates, there is less time for a sputtered droplet to form into a bigger droplet or debris on the surface before it is hit by the next laser beam; consequently, a finer appearance can be formed. Although the repetition rate has no significant impact on the ablated depth as discussed earlier, it should have noticeable influence on the morphology of the ablated surface.

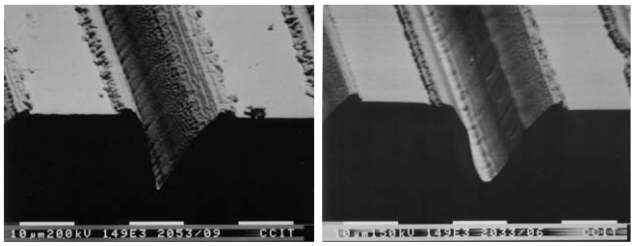

0.6 J-cm^{-2}, 5 Hz, 200 shots 1.4 J-cm^{-2}, 5 Hz, 200 shots

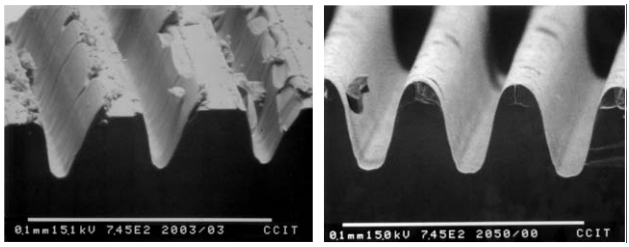

2.1 J-cm^{-2}, 5 Hz, 200 shots 2.4 J-cm^{-2}, 5 Hz, 200 shots

Fig. 15. Surface morphology and shape at different fluences.

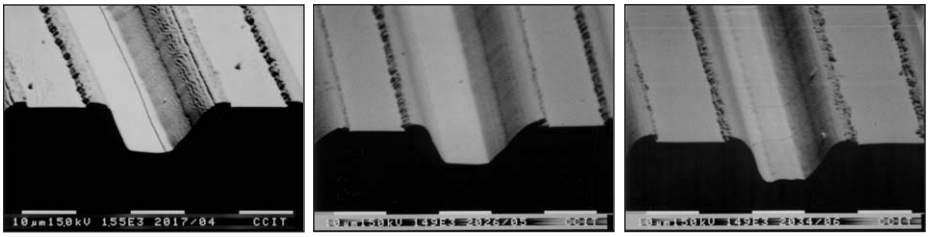

1.4 J-cm^{-2}, 1 Hz, 100 shots 1.4 J-cm^{-2}, 2 Hz/100 shots 1.4 J-cm^{-2}, 5 Hz, 100 shots

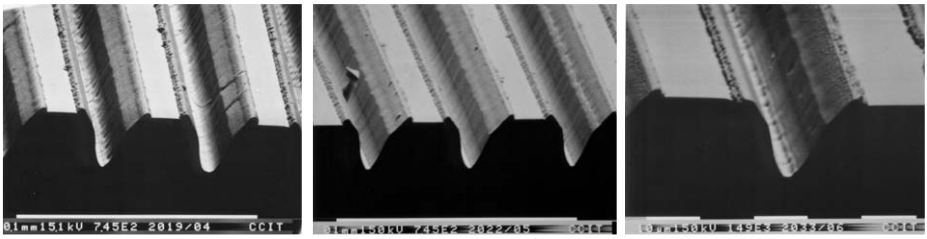

1.4 J-cm^{-2}, 1 Hz, 100 shots 1.4 J-cm^{-2}, 2 Hz/100 shots 1.4 J-cm^{-2}, 5 Hz, 100 shots

Fig. 16. Effect of repetition rate on surface morphology of ablated glass.

3.5. Ablation rate modeling

The laser ablation process, especially the pulse number and fluence effects on the ablation rate can be modeled analytically. It is assumed that the ablation process is

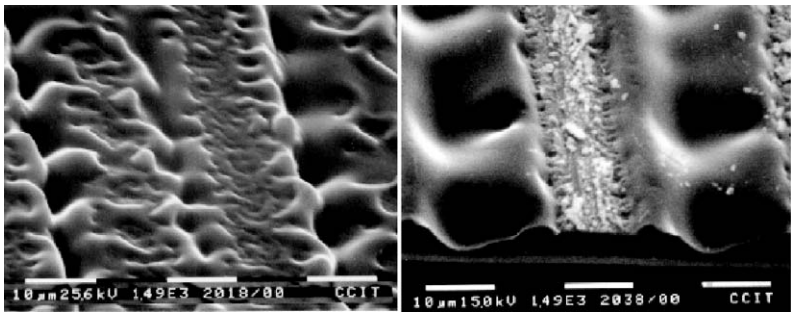

2.4 J-cm^{-2}, 1 Hz, 250 shots 2.4 J-cm^{-2}, 10 Hz, 250 shots

Fig. 17. Effect of repetition rate on surface morphology of ablated silicon.

dictated by a photothermal reaction that is similar to the present situation. A one-dimensional thermal conduction model previously developed for predicting laser heating and melting by Shen et al. [15] is modified for use in the present study. Basically, the propagation of the solid–liquid interface can be expressed by

$$S(t) = \frac{k_l}{A_l I}\left[\frac{2\lambda_l A_l^2 I^2}{k_l^2} t + C_0\right]^{1/2} \ln\frac{[2\lambda_l A_l^2 I^2 t/k_l^2]^{1/2}}{T_m} \quad \text{and}$$

$$C_0 = T_m^2 - \frac{\lambda_l k_s^2 A_l^2}{\lambda_s k_l^2 A_s^2}(T_m - T_0)^2, \tag{2}$$

where $S(t)$ is the position of the interface between the solid and the liquid phases, A_i, k_i and λ_i are the absorptivity, thermal conductivity and thermal diffusivity of the ith phase, respectively, with $i = s$ (solid phase) or l (liquid phase); I is the power density of the laser beam, and T_m and T_0 are the melting point and the ambient temperatures, respectively. Since the solution above does not consider the effect of latent heat during a phase change, it is not appropriate to apply this model to metals or other crystalline materials which possess large latent heat in a phase change. The borosilicate glass considered in the present research is not a crystalline material and thus has no phase change.

Using the material properties shown in Table 2, the analytical modeling of the four cases considered in Figs. 3–6 is performed. The material properties shown in Table 2 are obtained from the data in [8–11]. The absorptivity is estimated based on the data provided by the supplier. The analytical results are also plotted in the corresponding figures for comparison. As shown in the figures, the predicted ablation depth indeed grows as the number of pulses increases. This is consistent with the experimental observation. However, for all four cases compared, as the pulse number surpasses 100, the difference between the calculated and the experimental values increases. It is believed that this increasing discrepancy attributes to the fact that the one-dimensional model neglects the sidewall effects (the effects of the other two dimensions). The sidewall effects can be reasonably neglected with no significant errors at low pulse numbers because the ablated groove is still relatively shallow (as

shown in Fig. 13). On the other hand, at higher pulse numbers and fluences, the groove becomes deeper (as shown in Fig. 14) and the sidewall effects become significant. Thus, the one-dimensional heat transfer model is no longer reliable. The measured and calculated ablation depths are in closer agreement for laser pulses less than 150.

As shown earlier, the ablation depth increases linearly with the pulse number. Since the ablation depth represents the depth of either a V- or U-shaped groove, the ablated material or volume decreases as the groove becomes deeper or the width of the groove becomes narrower. In other words, the linear relationship between the ablation depth and the pulse number does not imply that the ablation volume increases linearly with the pulse number. For the sake of discussion, it is assumed that all of the ablated grooves become V-shaped after 250 pulses. The ablation depth measurements at a repetition rate of 5 Hz, as shown in Figs. 3–6, can be converted to ablated unit volume (volume per unit thickness), as shown in Fig. 18. It is obvious that the relationship between the ablated unit volume and the pulse number is no longer linear for the conditions considered. The analytical predications are also shown in curves in the figure. Since the analytical prediction is based on the one-dimensional solution, this implies that the width (span or mouth) of the groove is constant and the ablated unit volume is simply the product of the ablation depth and the constant width. As shown in the figure, the prediction of the ablated unit volume agrees well with the converted measurements. If the final groove cross sections are assumed to be U-shaped, the converted measurements will fall between those shown in Fig. 8 and those in Fig. 18. In either case, the agreement of the ablated volume cases is better than that of the ablation depth cases. One may also expect that if the groove is ablated deeper, the ablated volume rate should be lower. It is believed that

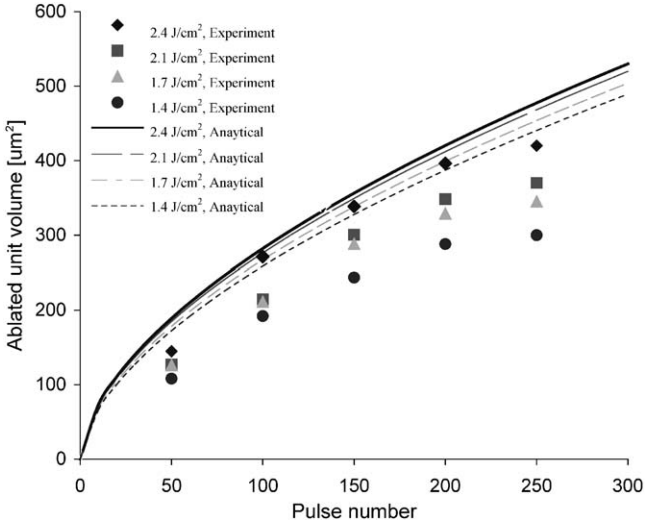

Fig. 18. Comparison of ablated unit volume between analytical predictions and measurements.

when the groove depth reaches a certain limit, the ablation volume rate may eventually decrease to an insignificantly small value.

4. Concluding remarks

A study using an excimer laser to machine high-aspect-ratio glass microstructures is presented and many fabrication issues that are often encountered in excimer projection ablation have also been addressed. The experimental study, using an ArF excimer laser, examines the ablation rates by varying several major operating parameters. The linear relationship between the ablation depth and pulse number has been identified. A similar relationship between the ablation depth and pulse fluence is also observed. Although the pulse repetition rate has no significant effects on the ablation depth, it has a noticeable impact on the morphology of the ablated surface. Results have indicated that increasing the repetition rate favors the morphology of ablated surfaces; however, sometimes the resulting debris or residue is hard to remove.

It is understood that the development of ablation processes relies on both theoretical and experimental investigations. In the theoretical portion, a simple analytical model is used to predict the ablation volume for comparison with the experimental measurements. A good agreement has been found between the prediction and the measured data on the ablated volume, but not on the ablated depth. Because the analytical model is based on a one-dimensional assumption, it does not accurately predict the profile variation of the ablated grooves. In the present study, it has been found that ablation at a relatively low fluence tends to form a V-shaped profile, while a U-shaped profile is ablated mainly at higher fluences.

The present study indicates that the materials of choice for excimer laser ablation should have low thermal conductivity and low melting temperature. Glass is one of the materials with these properties as compared to silicon and aluminum. The present study also indicates that the excimer laser micromachining system developed should be capable of making intricate glass-based microdevices to satisfy the needs of the photonics and communications industries. Furthermore, Further development in ablating intricate glass components should be encouraged.

In fact, by using multi-exposures of the mask present used and varying the focal length, the present technique can be extended to micromachine 3D structures. As an example, an optical probe array made at 1.2 J/cm^2 fluence is shown in Fig. 19. Currently, the use of the present system for fabricating other types of microstructures is under investigation. Moreover, for ablation of more intricate structures, a true three-dimensional numerical model should be developed to simulate the associated ablation phenomena. Non-thermal effects, including the photochemical effect, should also play a role in the ablation process; hence, some recent developments in modeling, such as those by Ho et al. [16] and Zhang et al. [17], could be considered and included for future modeling development.

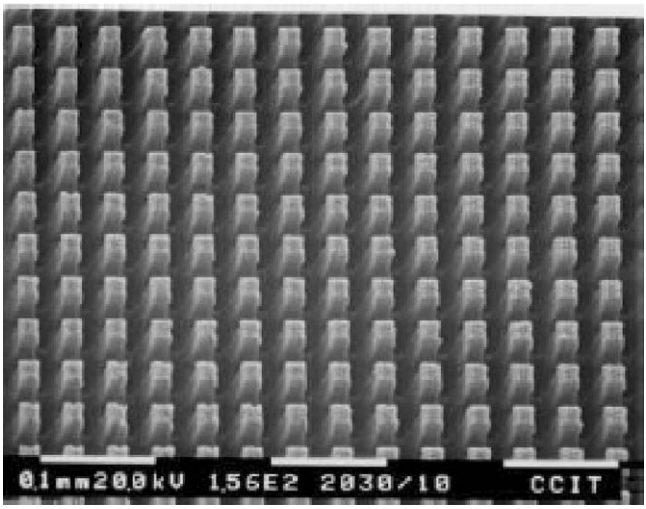

Fig. 19. Glass probe array micromachined by laser ablation.

Acknowledgements

The authors gratefully acknowledge the support of this study by the US National Science Foundation under Grant No. DMI-0002466 and CMS-0115828. A special thanks is to ROC National Science Council under Grant No. NSC90-2811-E-002-007 for providing funding for the first author to stay in Taiwan in 2001. The assistance from Mr. Jong-Seung Park of Arizona State University in computations should be specifically acknowledged.

References

[1] Metev SM, Veiko VP. Laser-assisted microtechnology. Berlin, Germany: Springer; 1994.
[2] Bado P, Clark W, Said A. Introduction to micromachining handbook. Ann Arbor, MI: Clark MXR, 2001. (also in http://64.227.154.50/Industrial/Handbook/Index.htm).
[3] Endert H, Patzel R, Basting D. Excimer laser: a new tool for precision micromachining. Opt Quantum Electron 1995;27:1319–35.
[4] Gu B, Hunter R, Wall D, Frechette M. Laser micromachining technology for device manufacturing. Med Device Diagn Ind 1998;12(11):62–8 (also in http://www.devicelink.com/mddi/archive/98/11/007.html).
[5] Duley WW. UV lasers: effects and applications in materials science. New York, NY: Cambridge University; 1996.
[6] Pãtzel R. An introduction to excimer lasers. In: Photonics handbook, 44th ed. Pittsfield, MA: Laurin Publishing, 2002. p. 247–52.
[7] Laude LD, editor. Excimer lasers. Dordrecht, Netherlands: Kluwer Academic, 1994.
[8] Boyer HE, Gall TL, editors. Metals handbook, Desk ed. Metal Park, OH: American Society for Metals, 1985.
[9] Bansal NP, Doremus RH. Handbook of glass properties. New York: Academic Press; 1986.

[10] Nikogosyan DN. Properties of optical and laser-related materials a handbook. New York, NY: Wiley; 1997.
[11] Kovacs TA. Micromachined transducers sourcebook. New York, NY: McGraw-Hill; 1998.
[12] Kautek W, Kruger J, Lenzer M, Sartania S, Spielmann C, Krausz F. Laser ablation of dielectrics with pulse duration 20 fs and 3 ps. Appl Phys Lett 1996;69(21):3146–8.
[13] Coleman HW, Steele WG. Experimentation and uncertainty analysis for engineers. New York, NY: Wiley; 1989.
[14] Rubahn HG. Laser applications in surface science and technology. New York, NY: Wiley; 1999.
[15] Shen ZH, Zhang SY, Lu J, Ni XW. Mathematical modeling of laser induced heating and melting in solids. Opt Laser Technol 2001;33:533–7.
[16] Ho JR, Grigoropoulos CP, Humphrey JAC. Computational study of heat transfer and gas dynamics in the pulsed laser evaporation of metals. J Appl Phys 1995;78(7):4696–709.
[17] Zhang W, Yao YL, Chen K. Modeling and analysis of UV laser micromachining of copper. Int J Adv Manufact Technol 2001;18(5):323–31.

Ampere A. Tseng is a Professor of Mechanical Engineering at Arizona State University. He was a recipient of the Superior Performance Award of Martin Marietta Laboratories, RCA Service Award, and Alcoa Foundation Research Award, and ASU 1999–2000 Faculty Award. Dr. Tseng was the Chair of the ASME Materials Division and of the 2000 NSF Workshop on Manufacturing of Micro-Electro-Mechanical Systems Workshop. Currently, Dr. Tseng is a fellow of ASME and the Chair of its Industrial Committee.

Ying-Tung Chen is an instructor of Mechanical Engineering at Chung Cheng Institute of Technology, Taiwan. He received his M.S. degree Chung Cheng Institute of Technology in May 2000. Currently, he is working on laser fabrication of three-dimensional microstructures.

K.J. Ma is an associate professor of Mechanical Engineering at Chung Hua University, Taiwan. He received his Ph.D. degree at the University of Birmingham (UK) in July 1997. After he returned from UK to Taiwan in September 1997, he worked for four years at Chung-Cheng Institute of Technology and set up excimer laser micromachining system. The research fields of Dr. Ma include surface modification of materials by various energy beams and biosensor fabrication.